Numerical modeling of Ce^{3+}-inhibitor release from novel corrosion protection coatings

Carlos Trenado[1,3]**, Matthias Wittmar**[1]**, Michael Veith**[1]**,
Nataly C Rosero-Navarro**[2]**, Mario Aparicio**[2]**, Alicia Durán**[2]**,
Yolanda Castro**[2] **and Daniel J Strauss**[1,3]

[1] INM-Leibniz Institute for New Materials, Campus D2 2, 66123 Saarbruecken, Germany
[2] Instituto de Cerámica y Vidrio (CSIC), Campus de Cantoblanco, 28049 Madrid, Spain
[3] Computational Diagnostics & Biocybernetics Unit, Saarland University Hospital, 66421 Homburg/Saar, Germany

E-mail: trenado@cdb-unit.de

Abstract
A novel hybrid sol–gel coating has recently been introduced as an alternative to high toxic chromate-based corrosion protection systems. In this paper, we propose a multiscale computational model to estimate the amount and time scale of inhibitor release of the active corrosion protection coating. Moreover, we study the release rate under the influence of parameters such as porosity and viscosity, which have recently been implicated in the stability of the coating. Numerical simulations obtained with the model predicted experimental release tests and recent findings on the compromise between inhibitor concentration and the stability of the coating.

S Online supplementary data available from stacks.iop.org/MSMSE/19/000000/mmedia

(Some figures in this article are in colour only in the electronic version)

AQ1

1. Introduction

Developing efficient and sustainable corrosion protection systems is one of the most challenging problems faced by today's metal industry. An important possibility for addressing this issue is provided by hybrid sol–gel coatings doped with inhibitors [1–3], in which the inhibitor release from the applied coating system enables active corrosion protection and self-healing. Such coatings may provide simultaneous active and passive corrosion protection in combination with additional desired surface properties without employing toxic heavy metal compounds.

To support the optimization and design of such coatings, we propose a multiscale model for the computational study of inhibitor release. Within this model, inhibitors are considered as ions, immersed in a sol–gel film (coating), which are subject to gradients of

concentration and potential [4, 5]. In contrast with previous models, we take into account capillary forces attributed to porous structures in the coating. Experimentally, such structures can be approached through ellipsometric porosimetry (EP), which allows the determination of the adsorption–desorption isotherms from the variation of refractive index and the thickness of the film induced by the change in the partial pressure of a solvent, in this case water. The pore-size distribution (PSD) can be obtained via porosimetry models usually based on the Kelvin equation. In addition, we emphasize the use of microdefect ionic measurements obtained by the scanning vibrating electrode technique (SVET), electrochemical measurements (polarization curves, electrochemical impedance spectroscopy (EIS)) and chemical characterization (SEM-EDS, FTIR) in order to define realistic initial and boundary conditions for the simulation of the self-healing process (inhibitor release) [4, 5]. An important consideration is that the process of self-healing involves multiple active scales with different physical and chemical processes, so it is crucial to use multiscale models. In particular, our modeling approach for self-healing involves a macroscale model of mass transport with embedded microscale relationships that incorporate effects at the particle scale.

2. Synthesis and characterization of coatings

A hybrid organic-inorganic sol was prepared from tetraethoxysilane (TEOS, ABCR 98%), 3-(methacryloxypropyl)trimethoxysilane (MPS, ABCR 98%), ethyleneglycol-dimethacrylate (EGDMA), glycidyl methacrylate (GM) and a colloidal silica suspension (LUDOX AS-40, aqueous suspension 40 wt%, particle size 5 nm, pH 9): 2,2′-Azobis (isobutyronitrile) (AIBN, Aldrich, 98%) was used as initiator of the free-radical organic polymerization. The sol, called TMEG–SiO$_2$, was prepared keeping the molar ratio TEOS/MPS/EGDMA of 62.5/25/12.5 and adding the colloidal silica suspension at a 35 mol% with respect to alkoxides. Ethanol absolute was added in order to obtain a silica concentration of $100 \, \text{g L}^{-1}$. The TMEG–SiO$_2$ sol was doped with Ce(NO$_3$)$_3$ · 6H$_2$O in an atomic ratio Si/Ce = 95/5 (TME–SiO$_2$–5Ce). Before coated, glass slide and AA2024 substrates were cleaned using absolute ethanol, an alkaline solution and a Turco Liquid Smugo-NC solution, respectively. Then, glass slides and AA2024 substrates were coated using the TMEG–SiO$_2$ and TME–SiO$_2$–5Ce sol's at withdrawal rates of 10 and $55 \, \text{cm min}^{-1}$. On the other hand, multilayer coatings were also prepared combining layers with and without cerium. In particular, a three-layer coating with the middle one containing cerium and the other two without was prepared. Coatings were dried at room temperature and sintered at 120 °C and 150 °C for 1 h with a heating rate of $10°\text{C min}^{-1}$. Each coating of the multilayer system was sintered at 120 °C for 1 h, the total multilayer thickness (the three layers together) being 9 μm [1, 2]. Cerium release tests were performed using the multilayer system on both substrates. Three samples with a total coated area of 41 cm^2 (each sample was coated in each one of its surfaces) were immersed vertically in three containers each with 50 ml of 3.5 wt% NaCl and maintained in solution for 1, 7 and 28 days. Each container was used for one immersion test. The cerium released to each solution was measured by inductively coupled plasma atomic emission spectroscopy (ICP-AES, Termo Jarrell Ash, IRIS model). The electrochemical behavior of the AA2024 and the multilayer coating was evaluated by potentiodynamic measurements after 1 h of immersion in 0.5 M of NaCl aqueous solution using a three-electrode cell. A saturated calomel and platinum electrodes were used as reference and counter-electrode, respectively. The potential was varied from −0.5 to 1.5 V with respect to the corrosion potential and the scan rate of $2 \, \text{mV s}^{-1}$. The working electrode area exposed was 1 cm^2. The tests were repeated three times for each immersion time in order to obtain a reliable estimate. The evolution of the refractive index and the thickness of TMEG–SiO$_2$ and TME–SiO$_2$–5Ce coatings were measured as a function of RH
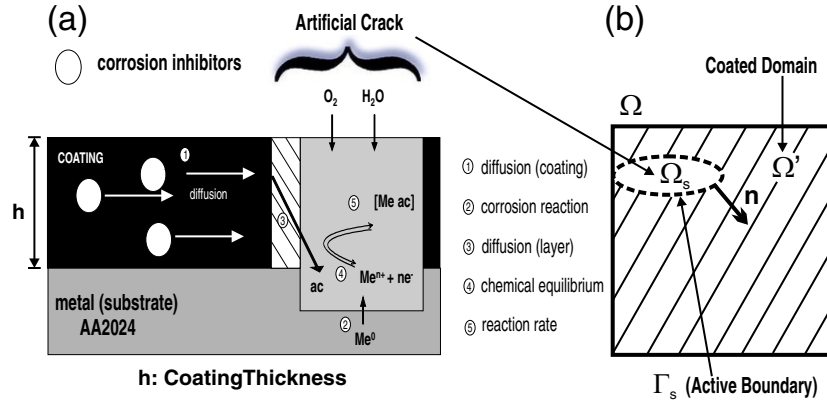
Figure 1. (*a*) lateral view of the coated substrate (AA2024) with an artificial crack; the corrosion and self-healing mechanisms considered in the model are indicated; (*b*) shows the domains involved in the model.

using a variable angle spectroscopic ellipsometer (Equipment Woollam M2000U) equipped with a humidity controlled chamber. An incidence angle of 70° was selected to perform the measurements.

3. Mathematical model of inhibitor release

We consider the following processes that are associated with the kinetics and thermodynamic mechanisms for self-healing and corrosion (figure 1(*a*)): (1) diffusion (coating), (2) corrosion reaction, (3) diffusion in the layer (scratch active boundary), (4) chemical equilibrium and (5) reaction rate. In the case of using AA2024 as a substrate, it is important to emphasize the presence of intermetallics as being active components in the formation of cathode–anode pairs when the system (coated substrate with artificial cracks) is exposed to an electrolyte solution [6]. In terms of our model, it is assumed that corrosion takes place at the cathode, while the anode represents a source of inhibitors. (See the supplementary material for details concerning the chemical reactions involved in the corrosion and the self-heling (re-passivation) mechanisms that are being considered in the model (stacks.iop.org/MSMSE/19/000000/mmedia)).

Let us denote by $c_i(\boldsymbol{x}, t)$ the concentration of participant species i (inhibitors and other reactive ions) at spatial location $\boldsymbol{x} \in \mathbb{R}^n (n = 1, 2, 3)$ and time $t \geqslant 0$, and $\Psi(\boldsymbol{x}, t) = \sum_{i=1}^{n} \Psi_{s_i}(\boldsymbol{x}, t)$ the net consumption of inhibitors (comprising the consumption at each scratch $s_i(i = 1, \ldots, n)$). We define the mass balance equation for species i in the domain $\Omega := \Omega_s \cup \Omega' \subset \mathbb{R}^n (n = 1, 2, 3)$ by

$$\frac{\partial c_i(\boldsymbol{x}, t)}{\partial t} + \nabla \cdot N_i = \Psi(\boldsymbol{x}, t) \qquad \text{on } \Omega \times (t_0, \infty) \tag{1}$$

$$c_i(x, t_0) = c_i^0 \qquad \text{on } \Omega \tag{2}$$

where $\Omega_s = \bigcup_{i=1}^{n} \Omega_{s_i}$ denotes the domain corresponding to possibly multiple scratches (Ω_{s_i}) present in the coating, $\Omega' = \Omega \setminus \Omega_s$ the undamaged (coated) domain (see figure 1(*b*)), $\frac{\partial}{\partial t}$ the partial differential operator with respect to t, ∇ the nabla operator, c_i^0 the concentration of species i at initial time t_0 and N_i the flux vector for species i defined by

$$N_i = -D_i \nabla c_i - z_i u_{m_i} F \nabla(c_i \nabla V) + F_\text{d}. \tag{3}$$

Here, D_i denotes the diffusivity, z_i the charge, and u_{m_i} the mobility of the ionic species i, F represents the Faraday constant, V the potential in the vicinity of a scratch s_i, and F_d a

Table 1. Nominal parameter values were obtained by fitting and from [1, 2, 5, 8, 9].

Parameter	Value	Units
F	96 485.339 9	$C\,mol^{-1}$
R	8.314 472	$JK\,mol^{-1}$
r	[5,15]	nm
h	[0.7,9]	μm
ϵ_p	[0,1]	Adimensional
$V_{corr}(AA2024)$	−0.55	V
μ	[5,35]	mP s
$\alpha_{m,M}$	[70°,95°]	Adimensional
$D_{eff}(Ce^{+3})$	$\approx 2.48 \times 10^{-7}$	$m^2\,s^{-1}$
$D(O_2)$	$\approx 2.15 \times 10^{-9}$	$m^2\,s^{-1}$
$D(OH^-)$	$\approx 5.1 \times 10^{-9}$	$m^2\,s^{-1}$
$D(H^+)$	$\approx 8.5 \times 10^{-9}$	$m^2\,s^{-1}$
$D(Na^+)$	$\approx 1.3 \times 10^{-9}$	$m^2\,s^{-1}$
$D(Cl^-)$	$\approx 1.7 \times 10^{-9}$	$m^2\,s^{-1}$

drag force that incorporates nanoporous effects. In particular, the mobility parameter can be calculated by the relationship $u_{m_i} = \frac{D_i}{RT}$, where R represents the universal gas constant and T denotes the temperature of the environment. By observing that the potential in the vicinity of a corroding cathode, located at x_0, is roughly characterized by a negative value with a slightly decreasing behavior in space, a generic potential function can be defined as $V(x) = V_{corr} + \exp(-x + x_0)$, where V_{corr} denotes the corrosion potential determined by potentiodynamic curves. Also, we assume that the drag force is directly proportional to the porous influence, so the following relationship is proposed: $F_d = \frac{\epsilon_p r^2}{\mu \tau} p_\mu$, where ϵ_p denotes the porosity, r the average radius of pores, μ the viscosity, τ the tortuosity of the porous media, and p_μ accounts for capillary forces. In order to account for such forces, that are associated with a random distribution of pores, we assume that the coating under study is divided into a sequence of patches of length δ, so that the capillary force is constant on each patch, namely $p_\mu(x) = \lambda_i$ for $x \in [x_k, x_{k+1}] \times [y_k, y_{k+1}]$ with $x_k = y_k = k\delta$ ($k = 1, 2, \ldots, n$), and λ_i is a uniform random variable such that $2\cos(\alpha_m) < \lambda_i < 2\cos(\alpha_M)$. Here α_m and α_M denote the minimum and maximum contact angles determined by the coating's inhibitor concentration under study (see data provided in the supplementary material (stacks.iop.org/MSMSE/19/000000/mmedia)). Here, we also point out that in each of the mentioned patches, uniformly distributed values for viscosity, porosity and radius of pores are assigned according to nominal intervals in (table 1).

With respect to the active boundary conditions, the molar fluxes of ionic species i at $\Gamma_{s_i} = \partial(\Omega_{s_i})$ (the boundary of scratch s_i) satisfy that $N_i \cdot n = \frac{\mu_{ij} I_j}{Fh}$, where n represents the normal vector to the boundary, μ_{ij} a stoichiometric coefficient for ionic species i in reaction j (corrosion and self healing kinetics), I_j is the ionic current density and h the coating thickness. At the cathode, the transition from an active (corrosive) state to a passive state, i.e. the self-healing process, is given by means of the ionic current $I_{j_{cathode}} = I_{j_{corr}} + I_{j_{inh}}$, where $I_{j_{corr}} = (1 - \alpha_p)I_{j_{corr,p}} + \alpha_p I_{j_{corr,a}}$, and $I_{j_{inh}} = (1 - \alpha_p)I_{j_{inh,p}} + \alpha_p I_{j_{inh,a}}$. Here, the subscripts corr and inh refer to ionic currents corresponding to corrosive and inhibiting species, a and p refer to active and passive states, and α_p is defined to be a sigmoid function with range between 0 and 1. In particular, we assume that a passive state is characterized by small and nearly constant ionic currents, while an active state by Butler–Volmer like-form ionic currents $I_{j_{corr,a}} = j_{0_I}\{e^{-\beta} - \frac{c_\alpha}{c_{0\alpha}}e^\beta\}$, $I_{j_{inh,a}} = j_{0_{II}}\{\frac{c_\gamma}{c_{0\gamma}}e^{-\delta} - e^\delta\}$, where β and δ represent cathodic and anodic Tafel constants, whereas $c_{0\alpha}$ and $c_{0\gamma}$ denote initial concentrations of corrosive and
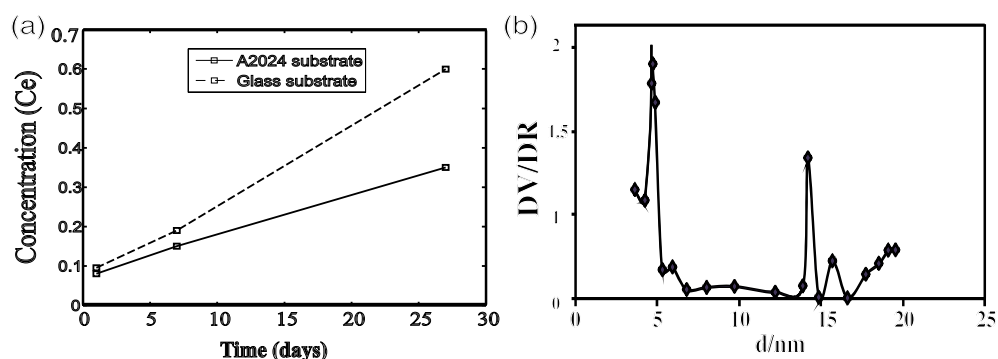
Figure 2. (*a*) Immersion tests corresponding to the TME–SiO$_2$–5Ce coating; (*b*) graph of the PSD of the coating in (*a*).

inhibiting species. We also suggest the use of an inhibitor effective diffusivity ($D_{eff}(Ce^{+3})$), resulting from host carrier effects, in accordance to the well-known Maxwell–Garnet theory [7]. For the numerical implementation of the model, the final element method defined on 1D and 2D multigrid meshes is required. In particular, the geometric multigrid solver of COMSOL, which provides a hierarchy of meshes in which discretized equations are evaluated on every level, is suitable for the non-linearities present in the equations. The advantage of geometric multigrid over algebraic multigrid solvers is apparent since non-linearities in the system are carried down to the coarse levels through the re-discretization. The kinetics of the process of corrosion can be incorporated via the COMSOL reaction engineering module.

4. Results and discussion

Homogeneous and crack-free coatings between 0.7 and 9 μm of thickness, depending on the concentration of the sol, were obtained by dip-coating onto glass slides and AA2024 substrates, with a good adherence after thermal treatment. A slight yellowish coloration was observed in the TMEG–SiO$_2$–5Ce coatings. Cerium release tests were performed to determine the cerium amount leached to the NaCl solution using two substrates: aluminum and glass. The results of Ce leaching (figure 2(*a*)) show an increase of the cerium released to the NaCl solution with the immersion time for both substrates. However, the glass substrate shows a higher cerium release compared with aluminum, increasing this difference with immersion time. At 28 days of immersion, 54 wt% and 36 wt% of Ce present in the coatings (1,1 mg) is leached to the solution from the glass and aluminum substrates, respectively. A possible explanation for this behavior is that on the aluminum substrate some cerium (from 18 wt% to 54 wt%) would be involved in sealing or healing these corrosion sites, indicating the participation of Ce in the corrosion processes, as also supported by our numerical simulations (figure 4(*a*)). Figure 3 shows the polarization curves for the multilayer coating compared with the bare AA2024. The presence of the coating improves the corrosion resistance of the aluminum. The corrosion current density decreased in four orders of magnitude from 10×10^{-3} to 10×10^{-8}–10×10^{-9} A cm^{-2}, observing a passivation range higher than 1 V. Ellipsometric measurements were used to evaluate the thickness and the refraction index of TMEG–SiO$_2$ and TMEG–SiO$_2$–5Ce coatings deposited on glass slides and sintered at 120 °C/1 h varying the relative humidity of water from 1 to 100%. For both coatings, when RH increases, the ellipsometric spectra change sharply and the fitting of the spectra becomes very difficult. This change of behavior can be attributed to the low sintering temperature and the high organic content of the coatings. In
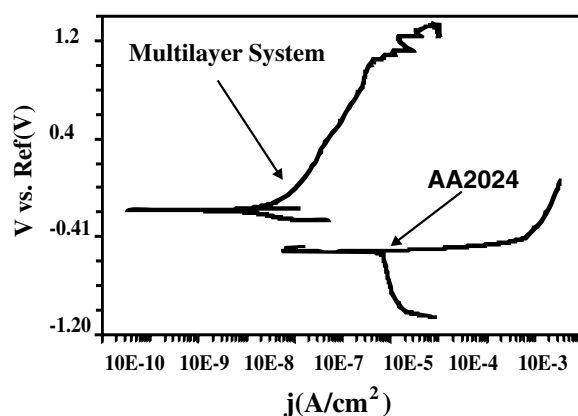
AQ2

Figure 3. Polarization curves corresponding to the coated sample (Multilayer System) and AA2024 (uncoated sample).

this respect, the swelling tendency of organic coatings with RH increments is well known as this method was developed for inorganic coatings. Therefore, TMEG–SiO$_2$ and TMEG–SiO$_2$–5Ce coatings were prepared and sintered at 150 °C/1 h for a better consolidation of the network. The adsorption isotherm was analyzed using the Bruggeman effective medium approximation (BEMA) model, considering the TMEG–SiO$_2$ coating as a reference. This material was used to simulate the contraction behavior of TMEG–SiO$_2$-Ce coatings and to determine the thickness of water adsorbed on the surface of the coating (the t-plot), considered equivalent to the adsorption behavior at the porous surface. By applying the Kelvin equation, the PSD was calculated from the adsorption branch (figure 2(*b*)). With respect to the determination of values for the variables j_{0_I} and $j_{0_{II}}$ and the concentrations $c_{0\alpha}$ and $c_{0\gamma}$, the SVET was well suited for the spatio-temporal measurement of ionic fluxes and concentrations, particularly because of the well-defined separation of cathodic and anodic regions in the considered corrosion systems (see the supplementary material for SVET sample data (stacks.iop.org/MSMSE/19/000000/mmedia)). In order to gain information about the inhibitor release under the influence of porosity and viscosity parameters, we first considered a simplified 1D model (cathode–anode system) in which it was assumed that all the inhibitor sources are concentrated in the anode, while the cathode represented the corrosion region. Using the simplified model, numerical simulations were performed (figures 4 and 5). Here, we assumed an exponentially decaying function Ψ_{s_i} as the consumption reservoir. In these figures, the *x*-axis denotes the space between the cathode and anode ($0 \leqslant R \leqslant 0.06 \times 10^{-1}$ m), and the *y*-axis indicates the log of inhibitor concentration. The total simulation time was 10^7 s, while the time required for the initial migration of inhibitors was approximately 1.45×10^3 s (figure 4(*a*)). Also, in figure 4(*a*) it can be seen that the transport of more than 50% of inhibitors had occurred by approximately 10^6 s, consistent with the data provided by our leaching experiments (figure 2(*a*)). Focusing on this graph, we see that the reduction of inhibitor concentration in the vicinity of the cathode (left point) reflects its reaction with other species (consumption) while exerting control in the corrosion area. In particular, for the simulation depicted in figure 4(*a*), we assumed radius of pores varying uniformly between 5 and 15 nm, viscosity and porosity values varying between 12 mP s and 15 mP s, and 0.5 and 0.7, respectively, contact angles varying between 85° and 90°, as well as diffusion coefficients estimated by fitting algorithms for leaching experiments and nominal values (table 1). Here, we point out that in order to achieve proper control of corrosion, inhibitor transport must be ensured in a reasonable time scale. In such respect, the model was able to make an estimate of such time scale through parameters obtained experimentally, in
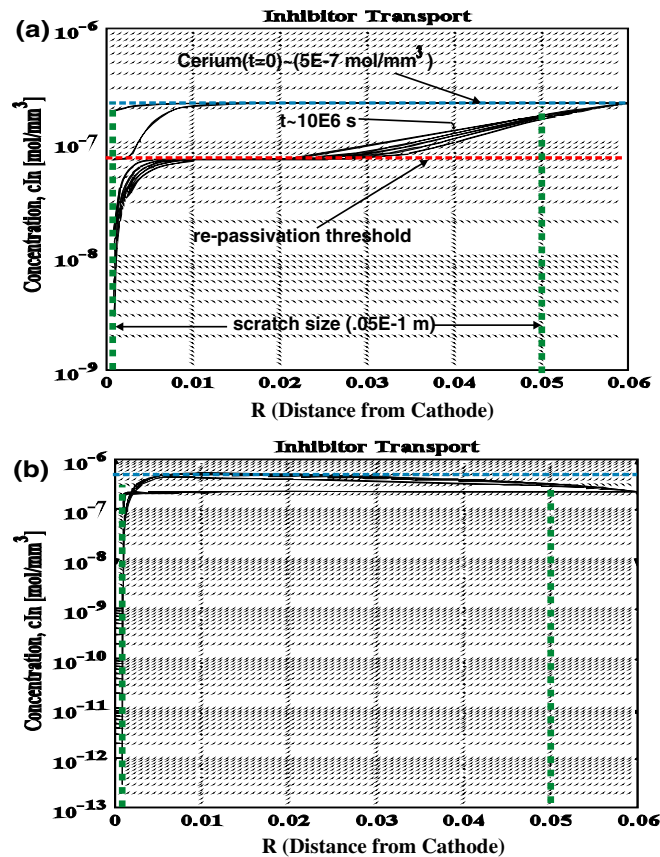
Figure 4. Results of simulations of the self-healing process obtained with the cathode–anode simplified model. The total simulation time was 10^7 s. In (*a*) nominal values of porosity and viscosity were used. As indicated, the initial Ce concentration is 5×10^{-7} mol mm^{-3} (blue line), the required time to achieve re-passivation is 10×10^6 s. The re-passivation threshold and scratch size (0.005 m) are indicated by red and green lines, respectively. In (*b*) nominal values of porosity and viscosity were decreased by 25%.

combination with fitted parameters as well as a hypothesized viscosity–porosity relationship. In figure 4(*b*) we show a simulation in which both the porosity and viscosity values were decreased by 25% in comparison with values in figure 4(*a*), resulting in poor transport and consumption of inhibitors. In figure 5(*a*) we show a simulation in which porosity was assumed as in figure 4(*a*), but the viscosity was decreased by 50%. In figure 5(*b*) we show a simulation in which both porosity and viscosity values were increased 40% in comparison with values used in figure 4(*a*). By setting parameter values as in table 1, and also including initial conditions provided by SVET, simulations were conducted in the domain shown in figure 6(*a*). In such a domain Ω with five microdefect domains Ω_{s_i} of sizes 4–5 mm, a multigrid mesh consisting of 61 184 elements was defined. In particular, mesh refinement at each microdefect was necessary for the optimization of the numerical scheme. Figure 6(*b*) corresponds to a time in which corrosion has already started in our simulation; figures 6(*c*)–(*f*) show the simulation of the self-healing process, confirmed experimentally [1, 2]. Corrosion control is clearly visible in the vicinity of every microdefect, reflected in an increase in inhibitor concentration over time, as shown in the figures. Here, the magnitude of the concentration is depicted by colors, namely black indicates a low concentration of inhibitors, while white indicates a high concentration.
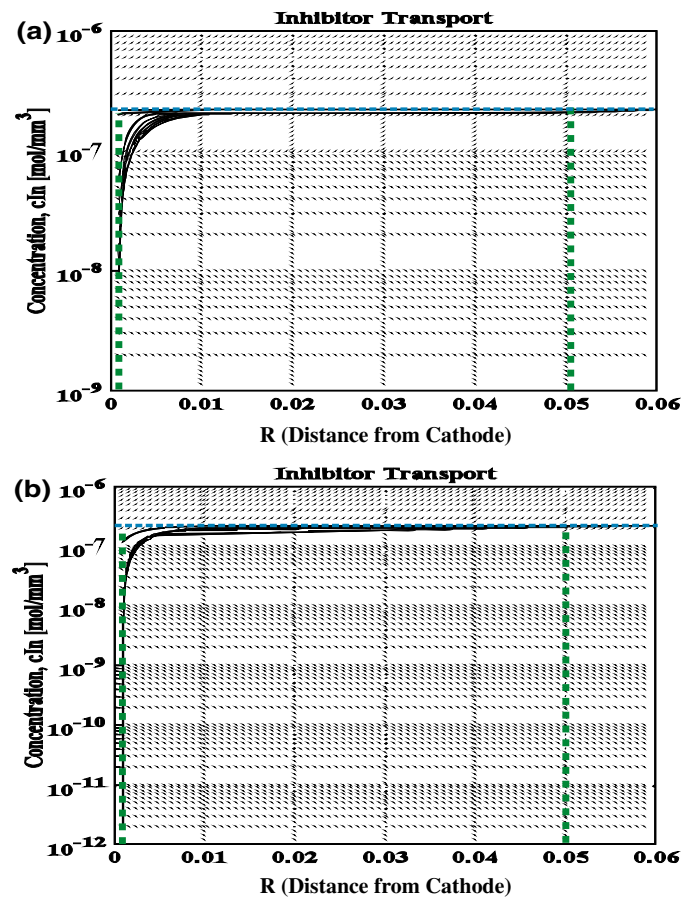
Figure 5. Results of simulations of the self-healing process obtained with the cathode–anode simplified model. The simulation time was 10^7 s. In (*a*) the porosity was maintained while the viscosity decreased by 50%. In (*b*) both parameters were increased 40% with respect to nominal values.

5. Conclusion

For the proposed coating, the amount and time scale of inhibitor release were computationally estimated. With respect to the effect of porosity and viscosity parameters on the inhibitor release, numerical simulations showed that higher (lower) values with respect to nominal ones for both of these parameters impair the release rate, whereas a decrease in the viscosity (porosity) by keeping the nominal porosity (viscosity) leads to a non-significant release. These results suggest that deviation of values for such parameters, with respect to nominal ones, has a critical influence on the release rate of inhibitors and thus the active corrosion protection. Furthermore, such results predicted recent findings on a relationship between optimal inhibitor concentration and the stability of the coating in relation to these parameters [8].

Although, the present study neither considers the dynamics of different electrolyte pH conditions nor addresses the important issue of the influence of scratch size into the inhibitor release. The proposed methodology represents a step ahead toward the study of structural properties of novel corrosion protection coatings in relation to their inhibitor release and self-healing capabilities.
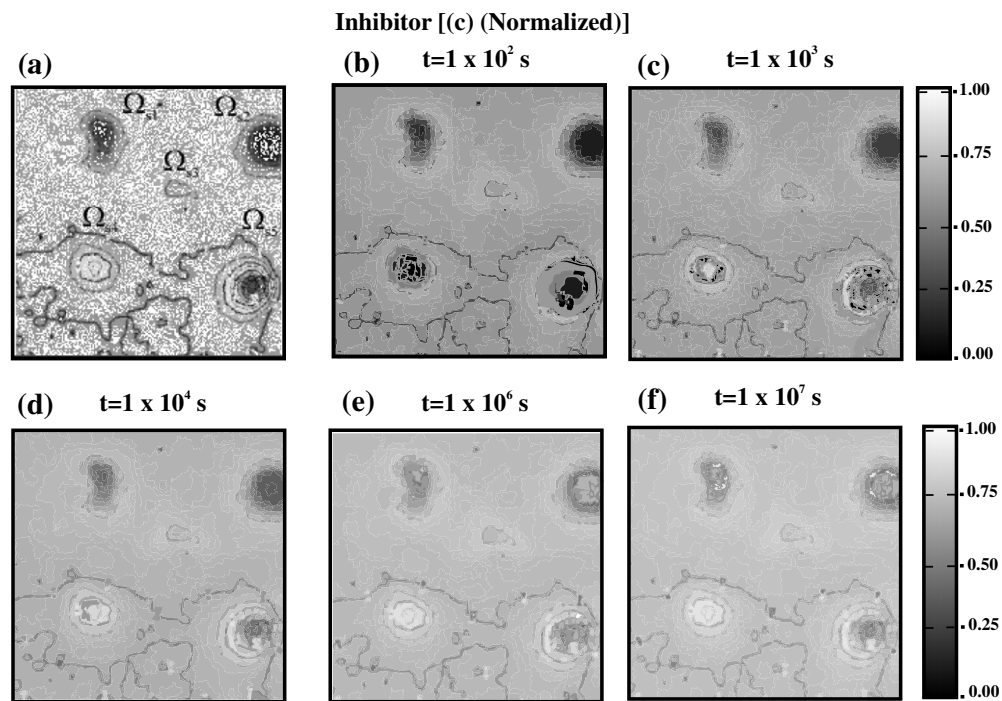
Figure 6. (*a*) shows a domain Ω with five microdefects (scratches) Ω_{s_i}; (*b*)–(*f*) show numerical simulations of the self-healing process provided by the proposed multifunctional coatings: (*b*) is at time in which corrosion has already initiated; that is, interaction of the electrolyte with the metal substrate and intermetallics through the microdefects initiate local chemical changes around each scratch; (*c*)–(*f*) show the effect of the migration of corrosion inhibitors (self-healing), as time passes there is an increase in inhibitor transport around each microdefect.

Acknowledgments

References

AQ3

[1] Rosero-Navarro N C, Pellice S A, Castro Y, Aparicio M and Durán A 2009 *Surf. Coat. Technol.* **203** 1879
[2] Rosero-Navarro N C, Pellice S A, Durán A and Aparicio M 2008 *Corros. Sci.* **50** 1283
[3] Surca Vuk A, Fir M, Jese R, Vilcnik A and Orel B 2008 *Prog. Org. Coat.* **63** 123
[4] Wang H, Presuel-Moreno F J and Kelly R G 2004 *Electrochim. Acta.* **49** 239
[5] Presuel-Moreno F J, Wang H, Jakab M A, Kelly R G and Scully J R 2006 *J. Electrochem. Soc.* **153** 486
[6] Yasakau K A, Zheludkevich M L, Lamaka S V and Ferreira M G S 2006 *J. Phys. Chem.* B **110** 5515
[7] Kalnin J R and Kotomin E 1998 *J. Phys. A: Math Gen.* **31** 7227
[8] Rosero-Navarro N C, Figiel P, Jedrzejewski R, Biedunkiewicz A, Castro Y, Aparicio M, Pellice S A and Durán A 2010 *J. Sol–Gel Sci. Technol.* **54** 301
[9] Rosero-Navarro N C, Paussa L, Andreatta F, Castro Y, Duran A, Aparicio M and Fedrizzi L 2010 *Prog. Org. Coat.* **69** 167